Optics Letters

Single-cycle pulse compression with over 20-fold peak power enhancement at an average power of 13.5 W

Yuzhe Liu[1,2] and Shaobo Fang[1,2,*]

[1] Institute of Physics, Chinese Academy of Sciences, Beijing 100190, China
[2] University of Chinese Academy of Science, Beijing 100049, China
*shaobo.fang@iphy.ac.cn

Received 6 June 2025; revised 23 July 2025; accepted 25 July 2025; posted 28 July 2025; published 28 August 2025

Intense single-cycle laser pulses serve as indispensable tools in disciplines such as strong-field physics and UV-IR spectroscopy. Traditional approaches for generating single-cycle pulses have encountered challenges in balancing high peak power, high average power, and high throughput efficiency. Here, we report the generation of 13.5-W, 3.7-fs single-cycle pulses with a peak power of 45.8 GW at a repetition rate of 50 kHz. By employing an argon-filled multi-pass cell and a single-pass compressor, we generated broadband white light spanning nearly two octaves. This approach achieved over 20-fold peak power enhancement and throughput efficiency of 67.5%. Our setup establishes an efficient methodology for producing single-cycle pulses from a common ytterbium laser, which simultaneously achieves high peak and high average power, facilitating many applications in ultrafast science.

https://doi.org/10.1364/OL.570102

Single-cycle pulses have garnered significant attention in strong-field applications, enabling unprecedented temporal resolution in diverse fields such as high harmonic generation (HHG) [1–4], isolated attosecond pulse generation [5–7], extreme ultraviolet pump-probe spectroscopy [8,9], and petahertz electronics [10–12]. To generate single-cycle pulses, both spectral broadening to over-octave-spanning bandwidth and precise dispersion compensation are indispensable. The single-cycle pulses were first achieved in Ti: Sapphire (Ti:Sa) laser [13–18]. By leveraging a 30-fs 1-kHz Ti:Sa laser, 2.6-fs pulses were achieved by Matsubara *et al*. through a two-step methodology: (1) white light generation via non-linear propagation in a gas-filled hollow-core fiber (HCF), and (2) fine-grained dispersion control using a spatial light modulator (SLM) [13]. Notably, the reduction in output peak power from 43 GW to 1.4 GW originates from the trade-off between (1) spectral broadening efficiency within the HCF and (2) energy loss during the sophisticated broadband dispersion control. By applying a multi-channel waveform synthesizer to pulses with an over-octave-spanning spectral range enabled the generation of single-cycle and sub-cycle pulses with 300 μJ of energy at a 3-kHz repetition rate [14,15]. This advanced synthesis process demanded precise control over both the intensity and relative phase of each spectral channel, ensuring coherent recombination of the ultra-broadband spectrum into transform-limited pulses. Thanks to advanced broadband dispersion coatings, simpler dispersion control can be achieved by combining chirped mirrors with materials featuring a high third-order dispersion (TOD)/group delay dispersion (GDD) ratio. Consequently, sub-3-fs pulses with hundreds of microjoules of energy can be compressed from supercontinuum generated via HCF or multi-thin plates (MTPs) [16–18]. However, the maximum attainable average power of single-cycle pulses from Ti:Sa laser is limited to below 1 W at repetition rates of several kHz. In contrast to Ti:Sa lasers, ytterbium (Yb) lasers offer distinct advantages in average power scalability and repetition rate scalability. Recent studies have demonstrated the generation of high-average-power few-cycle pulses using multi-pass cells (MPCs), MTPs, and HCFs [19–24]. Nevertheless, compressing pulses from a common Yb laser with typically hundreds of fs initial pulse durations to the single-cycle regime remains challenging.

Lately, limited attempts have been reported to achieve single-cycle pulse compression in Yb lasers [25–27]. By employing a two-stage MTP approach with pulse compression through an SLM in the 2nd stage, 3.2-fs pulses with 5 mW average power at 1 kHz were generated. The overall efficiency remained below 0.5%, and the peak power was reduced to 20% of its initial value, primarily constrained by the damage threshold of the SLM [25]. Using a two-stage HCF with waveform synthesizer-assisted pulse compression, a portion of the generated supercontinua (380–1000 nm) was compressed, causing the center wavelength of compressed pulses shifting to 736 nm with 13% throughput efficiency. The output yields 0.72 W, 2.1-fs pulses at a repetition rate of 6 kHz, with a peak power enhancement ratio of <10-fold [26]. The first demonstration of over 1 W average power for high-peak-power single-cycle Yb laser pulses was achieved through cascaded focusing and compression via four gas cells. With 1.34 mJ input pulse energy at 4 kHz, 3.9-W 3.1-fs pulses were generated, where chirped mirrors compensated for up to fifth-order dispersion. The peak power enhancement ratio reached 17-fold for this cascaded setup [27]. As summarized in Table 1,

Table 1. Comparison of Near-Single-Cycle Pulses Generation from Yb Laser

	[25]	[26]	[27]	Our Work
Repetition rate (kHz)	1	6	4	50
Average power (W)	0.005	0.7	3.7	13.5
Efficiency (%)	0.5	13	73	67.5
Output pulse duration (fs)	3.2	2.1	3.1	3.7
N of optical cycle	0.94	0.87	0.90	1.08

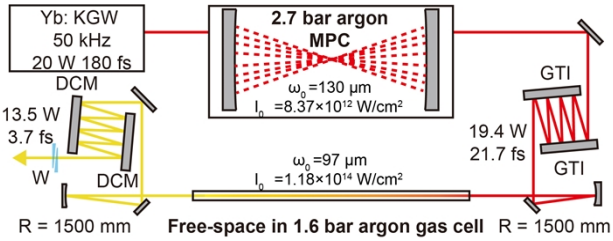

Fig. 1. Schematic diagram of the experimental setup. DCM, double-chirped mirror; GTI, Gires–Tournois interferometer mirror; W, wedge pairs; ω_0 and I_0 are the beam radius and peak intensity at the center of MPC and single-pass cell.

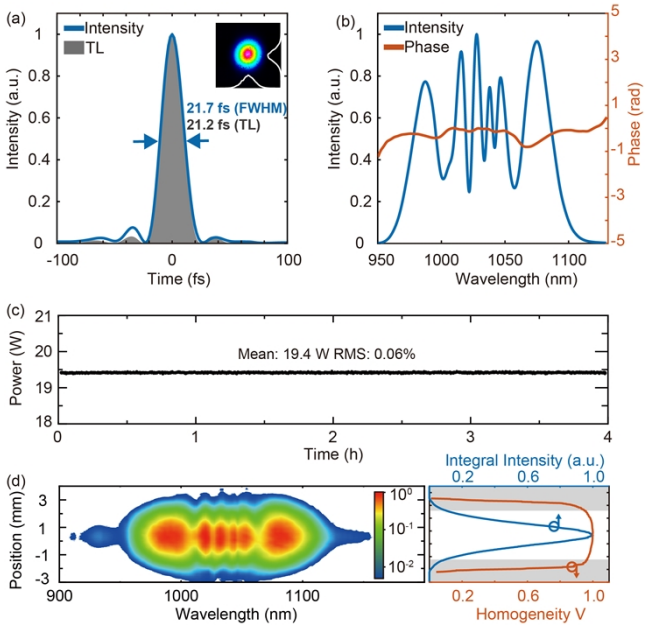

Fig. 2. Characterization of fundamental pulses after MPC. (a) Temporal intensity (blue line) along with transform limit (gray shadow), inserted figure: near-field beam profile. (b) Spectral intensity (blue line) and phase (red line). (c) Output power stability over 4 hours. (d) Spatio-spectral homogeneity with calculated V parameter (red line) along the integral intensity (blue line), gray shadow indicated the edge of $1/e^2$ intensity.

the aforementioned results universally required input pulse energy of 1 mJ and operated at a repetition rate of 1–6 kHz. In a recently developed soliton self-compression technique, single-cycle pulses were generated using a two-stage gas-filled antiresonant HCF [28]. Although this approach achieved 45-W average power, the 0.6-GW peak power still limits its applicability in strong-field physics. Consequently, all aforementioned schemes face the challenge of simultaneously achieving high peak power, high average power, high repetition rate, and high throughput efficiency. This is a critical bottleneck for fully exploiting the advantages of Yb lasers in the single-cycle regime.

In this Letter, we present the generation of 3.7 fs (1.08-cycle) pulses with 13.5 W average power at 50 kHz, resulting in 45.8 GW peak power and a throughput efficiency of 67.5%. The peak power is enhanced by a factor of 20.8. Driven by a 20-W, 180-fs Yb laser, we apply an argon-filled MPC to compress pulses from 180 fs to 21.7 fs, achieving an overall transmission of 97%. The near-transform-limited (TL) pulses yield 15.9 GW peak power, 19.4 W average power, and 0.06% long-term power stability over 4 hours. The compressed beam is focused into an argon-filled gas cell via free-space propagation. This white light generation process yielded a spectrum spanning 355–1285 nm, with the power fluctuation of 0.22%. Further fine-tuning of dispersion yielded 3.7 fs pulses (3.6 fs TL pulse duration), corresponding to 1.08 optical cycles at 1030 nm.

Our two-stage experimental setup consists of an argon-filled MPC and a gas cell (Fig. 1). Driven by a 20-W, 400-μJ, commercial Yb laser (Carbide, Light Conversion) operating at a 50-kHz repetition rate with 180 fs pulse duration, an argon-filled MPC (2.7-bar) is used to compress the fundamental pulses to 21.7 fs. A Galileo system ensures the beam diameter is adjusted to the eigenvalue (beam waist of 130 μm at focus) for spatially stable propagation between two concave mirrors (radius of curvature, ROC = 300 mm). The distance between the two mirrors is set to 58.2 cm, enabling 18 passes through the MPC. The adjusted eigenvalue results in the intensity of 8.4×10^{12} W/cm^2 at first focus in MPC. The uniformity of the beam profiles at the concave mirrors is verified by a CMOS-based beam profiler (LCM1310, DataRay) using the leaked light behind the concave mirror. The collimated beam after the MPC is compressed by two sets of GTI mirrors (Ultrafast Innovations, -200 fs^2 per bounce at 950–1120 nm; LAYERTEC, -100 fs^2 per bounce at 950–1120 nm, both reflectivity over 99.8% within 950–1120 nm), providing a total of -1400 fs^2 negative dispersion. The subsequent compression stage employs a 1-m-long gas cell (12 mm inner diameter) sealed with two broadband anti-reflection-coated 0.5-mm-fused silica windows. The output pulses from the MPC are focused into the gas cell by a concave mirror (ROC = 1500 mm). The white light generated in the gas cell is collimated by a silver-coated concave mirror with the same ROC. The collimated pulses are compressed by two sets of customized double-chirped mirrors DCMs (Ultrafast Innovations, providing -50 fs^2 GDD and over 94% reflectivity per bounce at 550–1450 nm), optimized for the wedge pair inside a D-scan system (Sphere Photonics). A total of 10 reflection bounces on the DCMs are implemented, where 6 bounces are designed to overcompensate the dispersion of the wedge pair.

The temporal and spectral characteristics of pulses after the MPC are measured using a SPIDER (APE). The compressed pulse duration is 21.7 fs, close to the TL pulse duration of 21.2 fs (Fig. 2(a)). This temporal profile shows that 89% of the energy is contained in the main lobe, resulting in a peak power of 15.9 GW with a Gaussian-distributed near-field beam profile (Fig. 2(a), inset figure). The broadened spectrum spans 950 nm to 1120 nm (Fig. 2(b)) with a quasi-flat phase. The average power of the compressed pulses is 19.4 W, yielding a transmission efficiency of 97%, which is higher than recent works [29–33]. The power stability of the compressed pulses is monitored with a high-precision power meter (Fig. 2(c)), show-

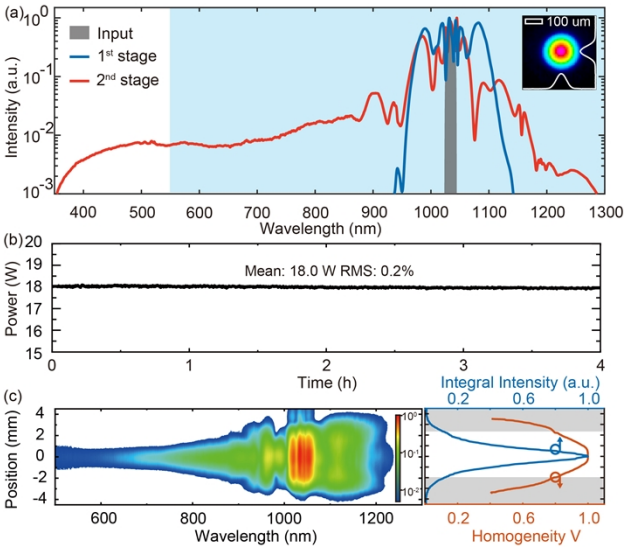

Fig. 3. Characterization of white light generation. (a) Output spectrum measured by an OSA (red line), compared with input spectrum before MPC (gray shaded area) and the output spectrum after MPC (blue line). Blue shaded area shows the spectral range for dispersion compensation. Inserted figure: the far-field beam profile focused by concave mirror (ROC = 1500 mm). (b) Output power stability over 4 hours. (c) Spatio-spectral homogeneity with calculated V parameter (red line) along the integral intensity (blue line), gray shadow indicated the edge of $1/e^2$ intensity.

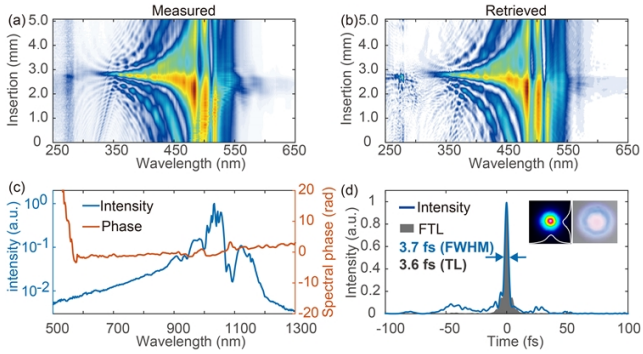

Fig. 4. Characterization of compressed single-cycle pulses. (a) Measured and (b) retrieved D-scan trance. (c) Spectral intensity (blue line) and the corresponding phase (red line). (d) Temporal intensity (blue line) and the corresponding TL intensity (gray shaded area). Inset figure: the near-field beam profile and the photography of the collimated beam.

ing a power fluctuation of only 0.06% over 4 hours. This value is almost identical to the laser's input power stability (0.06% over 4 hours). The spatio-spectral uniformity is measured by coupling the compressed pulses through a multi-mode fiber into a 100-μm pinhole at different positions. The spectra are recorded using an InGaAs-based spectrometer (D-vision, Sphere Photonics), and the results are plotted as a spectrogram along the beam profile (Fig. 2(d), left side). The integral intensity shows a Gaussian distribution (Fig. 2(d), blue line). The overlap parameter V is used to quantify the measurement result (Fig. 2(d), orange line), as calculated from previous reports [34,35]. The V parameter exceeds 96% across the recorded spectra within $1/e^2$ intensity radius (3.5 mm). The weighted mean value within the $1/e^2$ intensity region (Fig. 2(d), white area) is $V_{avg} = 99.5\%$, indicating excellent spectral overlap across the beam area. This compression stage yields a compression ratio of 8.3-fold and a peak power enhancement ratio of 7.2-fold.

The output spectrum from the free-space gas cell was recorded using an optical spectrum analyzer (OSA) (AQ6374E, Yokogawa) at 0.5 nm spectral resolution, revealing that the white light spanned 355–1285 nm at −30 dB, corresponding to an over 1.85 octave-spanning (Fig. 3(a)). The TL pulse duration over the full spectral range is 1.5 fs. Simulations are performed by solving the unidirectional pulse propagation equation based on the codes reported in [36]. Assuming radially symmetric free-space propagation, the beam radius at focus is 97 μm, resulting in peak power density at the focus of 1.18×10^{14} W/cm^2. However, the peak power density calculated in vacuum is 5.52×10^{13} W/cm^2, indicating a non-negligible self-focusing effect within the Rayleigh length of the focus, which is attributed to the peak power slightly surpassing the critical power of argon at 1.6 bar. As a result, a weak ionization area was created at about 680–800 mm from the focusing mirror. Using the Ammosov–Delone–Krainov (ADK) ionization model [37], we find that the maximum ionization rate within this area is 1.38×10^{-3}, occurring at 700 mm and 780 mm. This ebb and flow of ionization rate shows that a balance between self-focusing, plasma divergence, and diffraction is repeated twice in the gas cell. As a result, the plasma-induced refractive index changes and a frequency blue-shift occurs at the trailing edge of the pulse, as observed in Fig. 3(a). The output power fluctuation is 0.2% over 4 hours (Fig. 3(b)). The average power of the output pulses from the collimated beam is 18 W, corresponding to 93% efficiency in the white light generation process, mainly attributed to 20 μJ plasma absorption in the gas cell. To further verify the spatial uniformity of the output pulses under weak ionization, spatio-spectral uniformity measurement is performed using the same approach as in Fig. 2(d). The integrated intensity maintains a Gaussian distribution (Fig. 3(c), blue line). The V parameter exceeds 82% across the recorded spectra within $1/e^2$ intensity radius (4 mm). The weighted mean value of V parameter within $1/e^2$ intensity area (Fig. 3(c), white area) is $V_{avg} = 95.1\%$.

The temporal and spectral characteristics of the compressed pulses are measured using a D-scan. The measured and retrieved D-scan traces are depicted in Figs. 4(a) and 4(b). The retrieved spectral phase shows a flat phase from 550 nm to 1285 nm, with slightly high-order dispersion from 1000 nm to 1100 nm (Fig. 4(c)), which can also be observed from the D-scan trace. The retrieved temporal profile is 3.7 ± 0.1 fs for five measurements (Fig. 4(d)), close to TL pulse duration of 3.6 fs, corresponding to 1.08 optical cycles at 1030 nm. This temporal profile shows that 62.7% of the energy is contained in the main lobe. The photography and intensity distribution of the near-field beam show Gaussian-distributed white light within the $1/e^2$ beam area. The average power of the compressed pulses is 13.5 W, and the loss is mainly attributed to the ultra-broadband design of the DCMs, which undergo 10 reflection bounces, resulting in a final output peak power of 45.8 GW. The overall performance of our two-stage compressor is summarized in Table 2, which lists key parameters including pulse duration (τ_{FWHM}), TL pulse duration (τ_{TL}), pulse energy (E), transmission efficiency of each stage (η), average power (P_{avg}),

Table 2. Experimental Performance of Compressed Pulses at Each Stage Compared with Laser Input

	Input	1st Stage	2nd Stage
τ_{FWHM}(fs)	180	21.7	3.7
τ_{TL}(fs)	—	21.2	3.6
E(μJ)	400	388	270
η(%)	—	97	69.6
P_{avg}(W)	20	19.4	13.5
P_{stab}(%)	0.06	0.06	0.20
P_{peak}(GW)	2.2	15.9	45.8
V_{avg}(%)	–	99.5	95.1

power stability over 4 hours (P_{stab}), peak power (P_{peak}), and the weighted mean value of spatio-temporal overlap within $1/e^2$ intensity (V_{avg}). The final output yields an overall compression ratio of 48.6-fold and a peak power enhancement ratio of 20.8-fold, compared with the input pulses.

In conclusion, we achieved single-cycle pulse output with 13.5 W average power and a peak power enhancement of over 20-fold using a two-stage compressor. At the MPC stage, high-efficiency near-TL compression yielded 21.7 fs stable output with 19.4 W average power. A subsequent white light generation process resulted in spectral broadening from 355 nm to 1285 nm at −30 dB with 93% efficiency. The 18-W stable white light was then compressed by fine dispersion tuning over the 550–1285-nm range (Fig. 4(a), blue shaded area), delivering pulses with 13.5 W average power and 45.8 GW peak power. Argon was selected for the gas cell to minimize plasma diffusion time while maintaining a relatively high ionization potential compared to krypton [38]. As a result, our scheme allows for further scaling of the repetition rate. Unlike the MPC configuration, which requires peak power to remain below the critical power to maintain mode matching within the cavity [39], the single-pass configuration allows the peak power-to-critical power ratio (P_{peak}/P_{crit}) to exceed 1, which has been demonstrated in HCF systems [40]. Our approach further validates the feasibility and compressibility of free-space propagation at P_{peak}/P_{crit} ratios exceeding 1, alongside good spatio-spectral quality and power stability. Through a refined design of DCMs optimized for the 400–1300-nm spectral range with high-order dispersion management and higher reflectivity, the shorter pulses with peak power over 0.1 TW can be achieved. We believe that the presented single-cycle source can be replicated based on Yb lasers with similar input parameters. We foresee that this single-cycle source, combining high average power and high peak power, will serve as a powerful tool for strong-field physics, enabling efficient generation of intense extreme ultraviolet pulses and having a direct impact on the exploration of electron dynamics within the attosecond timescale.

Funding. Chinese Academy of Sciences Project for Young Scientists in Basic Research (YSBR-059); Beijing Natural Science Foundation for Distinguished Young Scholars (JQ22015).

Acknowledgment. S. Fang gratefully acknowledges support from Professor Mikio Yamashita and SECUF-D5.

Disclosures. The authors declare no conflicts of interest.

Data availability. Data underlying the results presented in this paper are not publicly available but may be obtained from the authors upon reasonable request.

REFERENCES

1. M. Yamashita, H. Shigekawa, and R. Morita, eds., in *Mono-Cycle Photonics and Optical Scanning Tunneling Microscopy: Route to Femtosecond Ångstrom Technology* (Springer, 2005), Vol. **99**.
2. M. Kretschmar, E. Svirplys, M. Volkov, *et al.*, Sci. Adv. **10**, eadk9605 (2024).
3. D. Nabben, J. Kuttruff, L. Stolz, *et al.*, Nature **619**, 63 (2023).
4. R. Weissenbilder, S. Carlström, L. Rego, *et al.*, Nat. Rev. Phys. **4**, 713 (2022).
5. E. Goulielmakis, M. Schultze, M. Hofstetter, *et al.*, Science **320**, 1614 (2008).
6. T. Gaumnitz, A. Jain, Y. Pertot, *et al.*, Opt. Express **25**, 27506 (2017).
7. J. Li, X. Ren, Y. Yin, *et al.*, Nat. Commun. **8**, 186 (2017).
8. M. Kretschmar, A. Hadjipittas, B. Major, *et al.*, Optica **9**, 639 (2022).
9. A. Zong, B. R. Nebgen, S.-C. Lin, *et al.*, Nat. Rev. Mater. **8**, 224 (2023).
10. C. Heide, P. D. Keathley, and M. F. Kling, Nat. Rev. Phys. **6**, 648 (2024).
11. D. A. Zimin, N. Karpowicz, M. Qasim, *et al.*, Nature **618**, 276 (2023).
12. A. Srivastava, A. Herbst, M. M. Bidhendi, *et al.*, Nat. Photonics **18**, 1320 (2024).
13. E. Substratum, K. Yamane, T. Sekikawa, *et al.*, J. Opt. Soc. Am. B **24**, 985 (2007).
14. A. Wirth, M. Th. Hassan, I. Grguraš, *et al.*, Science **334**, 195 (2011).
15. M. T. Hassan, T. T. Luu, A. Moulet, *et al.*, Nature **530**, 66 (2016).
16. H. Timmers, Y. Kobayashi, K. F. Chang, *et al.*, Opt. Lett. **42**, 811 (2017).
17. F. Silva, B. Alonso, W. Holgado, *et al.*, Opt. Lett. **43**, 337 (2018).
18. M. Seo, K. Tsendsuren, S. Mitra, *et al.*, Opt. Lett. **45**, 367 (2020).
19. Y. Liu, Z. Chen, S. Yang, *et al.*, Opt. Lett. **49**, 6992 (2024).
20. S. Goncharov, K. Fritsch, and O. Pronin, Opt. Lett. **49**, 2717 (2024).
21. T. Okamoto, Y. Kunihashi, Y. Shinohara, *et al.*, Opt. Lett. **48**, 2579 (2023).
22. Z. Pi, H. Y. Kim, and E. Goulielmakis, Opt. Lett. **47**, 5865 (2022).
23. A.-L. Viotti, C. Li, G. Arisholm, *et al.*, Opt. Lett. **48**, 984 (2023).
24. E. Shestaev, D. Hoff, A. M. Sayler, *et al.*, Opt. Lett. **45**, 97 (2020).
25. C.-H. Lu, W.-H. Wu, S.-H. Kuo, *et al.*, Opt. Express **27**, 15638 (2019).
26. Z. Pi, H. Y. Kim, and E. Goulielmakis, Optica **12**, 296 (2025).
27. M.-S. Tsai, A.-Y. Liang, C.-L. Tsai, *et al.*, Sci. Adv. **8**, eabo1945 (2022).
28. F. Köttig, D. Schade, J. R. Koehler, *et al.*, Opt. Express **28**, 9099 (2020).
29. M. Hanna, F. Guichard, N. Daher, *et al.*, Laser Photonics Rev. **15**, 2100220 (2021).
30. L. Silletti, A. Bin Wahid, E. Escoto, *et al.*, Opt. Lett. **48**, 1842 (2023).
31. M. Karst, M. Benner, P. Gierschke, *et al.*, Opt. Lett. **48**, 5899 (2023).
32. S. Hädrich, E. Shestaev, M. Tschernajew, *et al.*, Opt. Lett. **47**, 1537 (2022).
33. P. Balla, H. Tünnermann, S. H. Salman, *et al.*, Nat. Photonics **17**, 187 (2023).
34. V. Hariton, K. Fritsch, K. Schwarz, *et al.*, Opt. Express **31**, 19554 (2023).
35. J. Weitenberg, A. Vernaleken, J. Schulte, *et al.*, Opt. Express **25**, 20502 (2017).
36. C. Brahms and J. C. Travers, "Luna.jl: A flexible nonlinear optical pulse propagator," 1.1.0,Github 2024, https://github.com/Lupo-Lab/Luna.jl.
37. M. V. Ammosov, N. B. Delone, and V. P. Krainov, Sov. Phys. JETP **64**, 1191 (1986).
38. D. Schade, F. Köttig, J. R. Koehler, *et al.*, Opt. Express **29**, 19147 (2021).
39. M. Hanna, X. Délen, L. Lavenu, *et al.*, J. Opt. Soc. Am. B **34**, 1340 (2017).
40. G. Fan, P. A. Carpeggiani, Z. Tao, *et al.*, Opt. Lett. **46**, 896 (2021).